Int. J. Heat Mass Transfer. Vol. 36, No. 16, pp. 3957–3966, 1993
Printed in Great Britain

0017-9310/93 $6.00 + 0.00

Heatline visualization of forced convection laminar boundary layers

AL. M. MOREGA and A. BEJAN
Department of Mechanical Engineering and Materials Science, Duke University, Box 90300, Durham, NC 27708-0300, U.S.A.

(*Received* 16 *February* 1993 *and in final form* 19 *April* 1993)

Abstract—This paper reports in closed form the similarity heatfunctions H for laminar boundary layer flow on a flat wall. Plots of the constant-H lines ('heatlines') show that the path of convection from a hot free stream to a cold wall is unlike the path of convection from a hot wall to a cold fluid. The true path of convection in laminar boundary layer flow is visualized in charts drawn for both heat transfer modes (cold wall, hot wall), several Prandtl numbers (0.02, 0.72, 7) and isothermal walls and constant-flux walls. The paper stresses the heat transfer features that are brought into view for the first time by the heatline patterns. As a supplementary contribution, the paper reports the exact similarity solution for the wall with uniform flux in the $Pr \to 0$ limit, and proposes a closed-form local Nusselt number correlation that covers the entire Pr range.

1. INTRODUCTION

THE 'HEATLINE' method of visualizing the true path of convection heat transfer was proposed in refs. [1, 2]. It was developed as the convection counterpart (or the generalization) of the technique of heat flux lines used routinely in heat conduction.

The first application of heatlines was in the visualization of laminar natural convection in a two-dimensional rectangular enclosure heated from the side [1, 2]. The method has since been adopted and extended in several ways in the post-1984 literature. Littlefield and Desai [3] extended it to cylindrical coordinates and illustrated laminar natural convection in a vertical annular space. Trevisan and Bejan [4] defined the equivalent concept of masslines in convection mass transfer, and used it to visualize natural convection driven by concentration gradients in a two-dimensional rectangular enclosure. Morega [5] extended the method to the visualization of thermomagnetic convection in melts that are electrically conductive. Aggarwal and Manhapra [6] employed heatlines in a study of unsteady natural convection in a cylindrical enclosure. Heatlines were also used by Ho and Lin [7], who visualized the natural convection of cold water in a vertical annulus.

The interesting common feature of all the heatline patterns exhibited in the literature until now is that they refer to a single class of flows (natural convection in enclosures), which happen to be some of the most complicated forms of laminar convection known. If heatlines are to educate the eye to see the true path of the flow of energy through a convective fluid, then it makes even more sense to start exhibiting the heatlines of the simplest and most basic forms of convection heat transfer. The objective of this paper is to make this start. In it we present for the first time the heatlines of the classical (similarity) laminar boundary layer on a flat plate with uniform temperature or uniform heat flux.

2. ISOTHERMAL WALL WITH FORCED CONVECTION LAMINAR BOUNDARY LAYER

The equations that govern the conservation of mass, momentum and energy in the constant-property laminar boundary layer flow of Fig. 1 are (e.g. ref. [2], chap. 2):

$$\frac{\partial u}{\partial x}+\frac{\partial v}{\partial y}=0 \tag{1}$$

$$u\frac{\partial u}{\partial x}+v\frac{\partial u}{\partial y}=\nu\frac{\partial^2 u}{\partial y^2} \tag{2}$$

$$\rho c_{\mathrm{P}}\left(u\frac{\partial T}{\partial x}+v\frac{\partial T}{\partial y}\right)=k\frac{\partial^2 T}{\partial y^2}. \tag{3}$$

The heatfunction $H(x, y)$ for two-dimensional flow in Cartesian coordinates was defined in refs. [1, 2] for the more general case in which the longitudinal thermal diffusion term $k\,\partial^2 T/\partial x^2$ is not negligible in the energy equation. The special feature of the boundary layer simplified equation (3) is that the $k\,\partial^2 T/\partial x^2$ term is missing. This feature demands a special definition for the heatfunction $H(x, y)$ that is valid inside the boundary layer region:

$$\frac{\partial H}{\partial y}=\rho c_{\mathrm{P}} u(T-T_{\mathrm{ref}}) \tag{4}$$

$$-\frac{\partial H}{\partial x}=\rho c_{\mathrm{P}} v(T-T_{\mathrm{ref}})-k\frac{\partial T}{\partial y}. \tag{5}$$

The reference temperature T_{ref} is an arbitrary constant. In this paper we assign to this constant a precise

NOMENCLATURE

c_p	specific heat at constant pressure
f	Blasius function, equation (6)
g	similarity heatfunction, equation (13)
H	heatfunction
$\tilde{H}$	dimensionless heatfunction, equations (10), (27)
$\hat{H}$	dimensionless heatfunction, equation (34)
k	thermal conductivity
L	wall length
Nu	local Nusselt number, equation (31)
$\overline{Nu}$	overall Nusselt number, equations (23), (24)
Pr	Prandtl number
q''	wall heat flux
$\bar{q}''$	average heat flux
Re_x	Reynolds number, $U_\infty x/\nu$
T	temperature
T_{ref}	reference (lowest) temperature
T_0	wall temperature
T_∞	free stream temperature
u, v	velocity components, Fig. 1
U_∞	free stream velocity
x, y	Cartesian coordinates, Fig. 1
$\tilde{x}, \tilde{y}$	dimensionless coordinates, equation (9).

Greek symbols

α	thermal diffusivity
δ_{99}	velocity boundary layer thickness, $5x\,Re_x^{-1/2}$
ζ	similarity variable, equation (A2)
η	similarity variable, equation (8)
θ	similarity temperature profile, equation (10)
ν	kinematic viscosity
ρ	density
τ	similarity temperature profile, equation (A1).

meaning: T_{ref} is the *lowest* temperature in the boundary layer region. We begin with the case where the free stream is warm and the wall is cold, $T_\infty > T_0$, which means that $T_{ref} = T_0$. Later we shall consider the reverse situation in which the wall is warmer than the stream.

It is easy to verify that the function $H(x, y)$ defined by equations (4) and (5) satisfies the energy equation (3) identically. The challenge is to find this function by using equations (4) and (5). The boundary layer flow field is described by the classical Blasius solution (e.g. ref. [2], p. 48),

$$u = U_\infty f' \tag{6}$$

$$v = \frac{1}{2}\left(\frac{\nu U_\infty}{x}\right)^{1/2}(\eta f' - f) \tag{7}$$

where $f' = \mathrm{d}f/\mathrm{d}\eta$, and

$$\eta = \frac{y}{x} Re_x^{1/2}, \quad Re_x = \frac{U_\infty x}{\nu}. \tag{8}$$

For the calculations described in this paper, we determined the Blasius function $f(\eta)$ using the following method. We wrote the Blasius equation as a first-order autonomous system of ordinary differential equations and solved it using a variable (adaptive) step, 4th/5th order Runge–Kutta scheme with error control per time step and 10^{-6} tolerance over the $0 \leqslant \eta \leqslant 500$ interval. The unknown value of $f''(0)$ was found through a trial-and-error shooting technique.

It is convenient to restate the heatfunction problem in terms of the following dimensionless variables:

$$\tilde{x} = \frac{x}{L}, \quad \tilde{y} = \frac{y}{L\,Re_L^{1/2}} \tag{9}$$

$$\theta = \frac{T - T_0}{T_\infty - T_0}, \quad \tilde{H} = \frac{H}{\rho c_p U_\infty (T_\infty - T_0) L\,Re_L^{-1/2}} \tag{10}$$

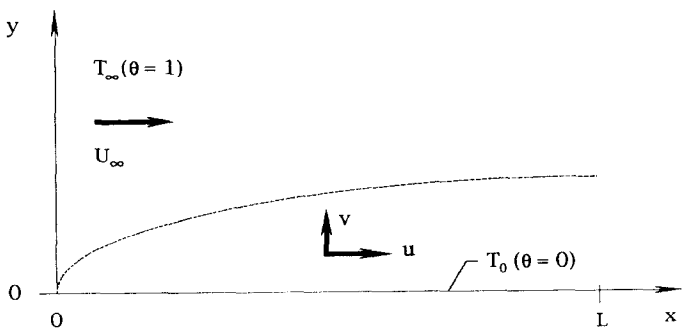

FIG. 1. The laminar boundary layer over a flat plate parallel to the free stream.

in which $Re_L = U_\infty L/\nu$. By using these definitions and the Blasius flow solution (6)–(8), the heatfunction gradients (4) and (5) become

$$\frac{\partial \tilde{H}}{\partial \tilde{y}} = f'\theta \tag{11}$$

$$-\frac{\partial \tilde{H}}{\partial \tilde{x}} = \tfrac{1}{2}\tilde{x}^{-1/2}(\eta f' - f)\theta - \frac{1}{Pr}\frac{\partial \theta}{\partial \tilde{y}}. \tag{12}$$

In these equations Pr is the Prandtl number, η is equal to $\tilde{y}\tilde{x}^{-1/2}$ and the function $\theta(\eta, Pr)$ is the similarity temperature profile obtained by Pohlhausen (e.g. ref. [2], p. 51). We computed $\theta(\eta)$ and $\theta'(\eta)$ for each Pr value using an adaptive Gauss quadrature implemented by MATHEMATICA®. We set to 16 digits the working precision and to 10^{-8} the accuracy goal of the numerical integration. The intermediate $f(\eta)$ values needed for the $\theta(\eta)$ integration were deduced from the discrete Blasius solution (f, f', f'') by using a locally parabolic interpolation procedure. The 10^{-6} error limit was preserved throughout the numerical process.

Like the temperature field of the Pohlhausen solution, the heatfunction field depends on the Prandtl number. The derivation of the analytical form of the dimensionless heatfunction $\tilde{H}(\tilde{x}, \tilde{y})$ begins with assuming

$$\tilde{H}(\tilde{x}, \tilde{y}) = \tilde{x}^{1/2} \cdot g[\eta(\tilde{x}, \tilde{y})] \tag{13}$$

and rewriting equations (11) and (12) in terms of the unknown function $g(\eta)$

$$g' = f'\theta \tag{14}$$

$$\eta g' - g = (\eta f' - f)\theta - \frac{2}{Pr}\theta' \tag{15}$$

where $g' = \mathrm{d}g/\mathrm{d}\eta$. By eliminating g' between equations (14) and (15) we obtain

$$g(\eta) = f\theta + \frac{2}{Pr}\theta'. \tag{16}$$

The analytical form of the boundary layer heatfunction is therefore

$$\tilde{H}(\tilde{x}, \eta) = \tilde{x}^{1/2}\left[f(\eta)\theta(\eta) + \frac{2}{Pr}\theta'(\eta)\right]. \tag{17}$$

Along the wall the $\tilde{H}$ values increase as $\tilde{x}^{1/2}$,

$$\tilde{H}(\tilde{x}, 0) = \frac{2}{Pr}\theta'(0)\tilde{x}^{1/2} \tag{18}$$

because $\theta'(0)$ is only a function of Pr (e.g. ref. [2], pp. 51–52)

$$\theta'(0) = 0.332\, Pr^{1/3} \quad (Pr > 0.5) \tag{19}$$

$$\theta'(0) \to 0.564\, Pr^{1/2} \quad (Pr \ll 0.5). \tag{20}$$

The wall heatfunction is zero at the tip of the boundary layer. At the downstream end of the wall ($\tilde{x} = 1$) the heatfunction reaches its highest value, which is $2\theta'(0)/Pr$. This value is proportional to the total heat transfer rate absorbed by the wall. Note the factor of 2 in front of $\theta'(0)$ and the limiting values

$$\tilde{H}(1, 0) = 0.664\, Pr^{-2/3} \quad (Pr > 0.5) \tag{21}$$

$$\tilde{H}(1, 0) \to 1.128\, Pr^{-1/2} \quad (Pr \ll 0.5). \tag{22}$$

The factors 0.664 and 1.128 are the same as in the expressions for the overall Nusselt number,

$$\overline{Nu} = 0.664\, Pr^{1/3}\, Re_L^{1/2} \quad (Pr > 0.5) \tag{23}$$

$$\overline{Nu} = 1.128\, Pr^{1/2}\, Re_L^{1/2} \quad (Pr \ll 0.5) \tag{24}$$

where $\overline{Nu} = \bar{h}L/k$ and $\bar{h} = \overline{q''}/(T_\infty - T_0)$. Over the entire Pr range the relationship between $\overline{Nu}$ and the $\tilde{H}$ value at the trailing edge is

$$\overline{Nu} = \tilde{H}(1, 0)\, Pr\, Re_L^{1/2} \tag{25}$$

which is equivalent to

$$\overline{q''}L = H(x = L, y = 0). \tag{26}$$

In conclusion, the physical (dimensional) value of the trailing-edge heatfunction is equal to the toal heat transfer rate through the wall. The analytical form of the function $g(\eta)$ found in equation (16) shows that the heatfunction accounts simultaneously for the two heat transfer mechanisms that are present in the boundary layer, convection ($f\theta$) and transversal conduction ($2\theta'/Pr$). The $g(\eta)$ function is the similarity profile of the boundary layer: g is as basic a feature of the similarity boundary layer as f and θ.

3. THE HEATLINES NEAR A COLD ISOTHERMAL WALL

Figure 2 shows the pattern of heatlines in the boundary layer region of a $Pr = 0.72$ fluid such as air. The boundary layer region is drawn in terms of $\tilde{x}$ vs η, with η as large as 5 so that u approaches 99% of

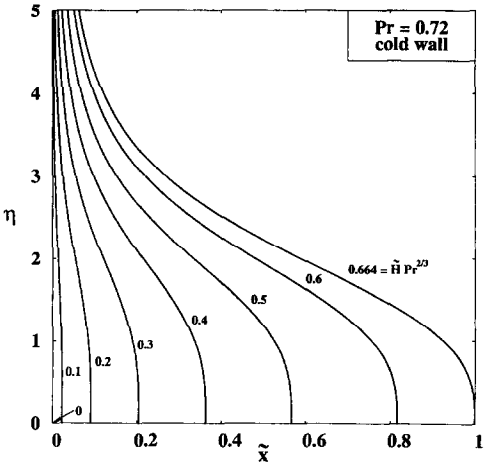

FIG. 2. The heatlines in the scaled boundary layer of thickness $0 \leqslant \eta \leqslant 5$, when the isothermal wall is colder than the free stream ($Pr = 0.72$).

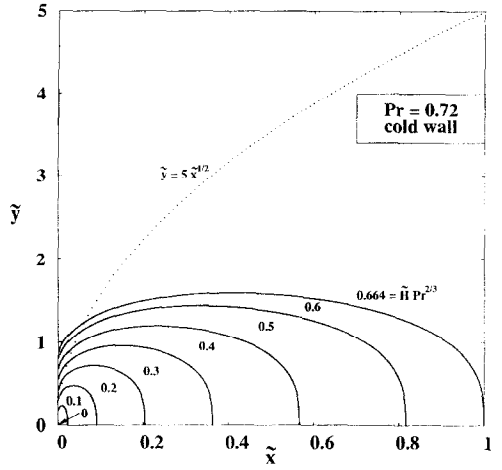

FIG. 3. The heatlines near a cold isothermal wall ($Pr = 0.72$).

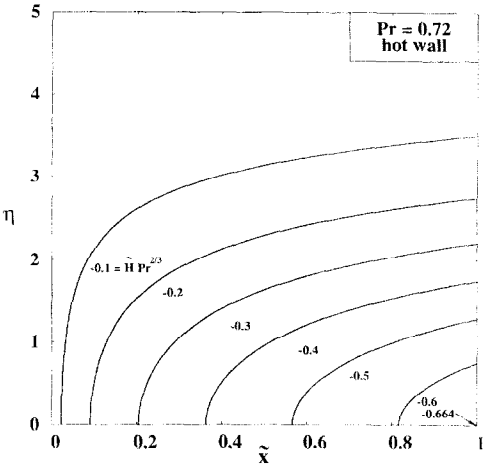

FIG. 4. The heatlines in the scaled boundary layer of thickness $0 \leqslant \eta \leqslant 5$, when the isothermal wall is warmer than the free stream ($Pr = 0.72$).

the free stream value U_∞. The heatlines are drawn for constant values of $\tilde{H}\,Pr^{2/3}$ in accordance with equation (21), i.e. for the purpose of showing that the $\tilde{H}\,Pr^{2/3} = 0.664$ line passes through the trailing edge of the wall.

The same heatlines are shown in Fig. 3, this time in the corresponding Cartesian frame of $\tilde{x}$ vs $\tilde{y}$. The heatlines are plotted only in the boundary layer region, which corresponds to $\tilde{y}$ values where $\eta < 5$. The $\eta = 5$ curve (or $\tilde{y} = 5\tilde{x}^{1/2}$) is shown by the dotted line: it represents the velocity boundary layer, or a thickness that is approximately the same as δ_{99} [8].

The heatlines show the actual path of the energy absorbed by the wall. They are perpendicular to the wall because at $\tilde{y} = 0^+$ the heat transfer is by pure conduction and the wall is an isotherm. The heatlines that ultimately cross the wall ($0 < \tilde{H}\,Pr^{2/3} < 0.664$) originate from the flow region situated immediately upstream of the tip. Note that when the heatlines enter the boundary layer region they are tilted away from the cold wall. Their direction turns toward the wall, which they eventually cross. This change in direction occurs, approximately, at the half-point of the distance between the tip and the point where the heatline enters the wall.

The heatlines that cross the wall are more crowded near the tip than farther downstream. This feature of the heatline pattern makes visible the nonuniform distribution of the heat flux over the isothermal wall, namely a heat flux q'' that is proportional to $x^{-1/2}$.

4. THE HEATLINES NEAR A HOT ISOTHERMAL WALL

Consider now the reverse situation in which T_0 is greater than T_∞, and the wall heats the stream. The temperature field is insensitive to this change (note that in both situations $\theta = 0$ on the wall, and $\theta = 1$ in the free stream, Fig. 1), however, the pattern of heatlines is markedly different. This drastic change in the heatline pattern should be expected because in Fig. 3 the wall served as heat sink, while now it is the heat source.

The analytical construction of the $\tilde{H}$ function begins with setting $T_{ref} = T_\infty$ in equations (4) and (5), and follows the steps and definitions outlined in Section 2. For the sake of conciseness we list only the final expression for the dimensionless heatfunction:

$$\frac{H}{\rho c_p U_\infty (T_0 - T_\infty) L\, Re_L^{-1/2}} = \tilde{H}(\tilde{x}, \tilde{y}) = -\tilde{x}^{1/2}\left\{ f(\eta)[\theta(\eta) - 1] + \frac{2}{Pr}\theta'(\eta) \right\}. \quad (27)$$

Compare this $\tilde{H}$ definition with that of equation (10), and note the use of the positive temperature difference $T_0 - T_\infty$ in the current denominator. The dimensionless heatfunction $\tilde{H}$ decreases as we sweep the wall in the flow direction (e.g. Figs. 4 and 5), because the hot wall releases energy into the fluid. When the wall is colder than the fluid, the heat function $\tilde{H}$ of equa-

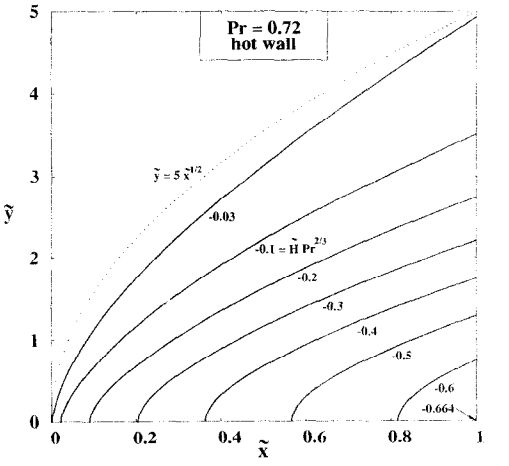

FIG. 5. The heatlines near a hot isothermal wall ($Pr = 0.72$).

tions (10) increases in the x direction (Fig. 3) because the wall absorbs energy.

Figures 4 and 5 show the pattern of heatlines near the hot wall, when the Prandtl number is 0.72. These figures must be compared with Figs. 2 and 3 to see the difference between a wall that releases heat and one that absorbs heat. Figure 4 shows the heatlines in the scaled boundary layer region $0 \leqslant \eta \leqslant 5$, while Fig. 5 shows the same pattern in the corresponding Cartesian frame. The heatlines point in the $\tilde{y}$ direction as they emerge from the wall; later, they are swept downstream by the flow. Their higher density near the tip indicates higher heat fluxes. They occupy the same region as the velocity boundary layer (the dotted line) and in this way they visualize the meaning of a Prandtl number that is of the order of 1.

The $Pr \sim 1$ property is illustrated further by the heatline that originates from the tip of the plate ($\tilde{H}\, Pr^{2/3} = 0$). This outermost heatline almost coincides with the edge of the velocity boundary layer. In Fig. 5 we had some difficulty plotting exactly the tip heatline $\tilde{H}\, Pr^{2/3} = 0$, and settled for one that originates from sufficiently close to the tip, $\tilde{H}\, Pr^{2/3} = -0.03$. This difficulty is due to the fact that $\eta \to \infty$ as $\tilde{x} \to 0$. The $\tilde{H} \to 0$ heatlines near the $\tilde{x} \to 0$ region were plotted after rewriting equation (27) as

$$\tilde{H}(\tilde{x}, \eta) = -\tilde{y}\left\{\frac{f(\eta)[\theta(\eta)-1]}{\eta} + \frac{2}{Pr}\frac{\theta'(\eta)}{\eta}\right\}. \qquad (27')$$

In order to avoid numerical overflows, we used asymptotic expansions for $\tilde{H}$, instead of the interpolating scheme outlined in Section 2.

5. THE PRANDTL NUMBER EFFECT ON THE HEATLINE PATTERN

We repeated the construction of $\tilde{H}$ patterns for several Pr values, large and small. Figures 6 (cold wall) and 7 (hot wall) correspond to $Pr = 7$ (e.g. water). If we compare them with the $Pr = 0.72$ patterns of Fig. 3 and, respectively, Fig. 5, we see very clearly that the region occupied by the heatlines becomes thinner than the velocity boundary layer as the Prandtl number increases. Specifically, the thickness of the heatline pattern appears to decrease by a factor of about 1/2, while Pr changes from 0.72 to 7. This agrees very well with the proportionality that exists between the scale of the thermal boundary layer thickness and $Pr^{-1/3}$ (when $Pr \geqslant 1$) (e.g. ref. [2], p. 38): for the change from $Pr = 0.72$ to $Pr = 7$ this proportionality recommends a decrease by nearly the same factor, $(7/0.72)^{-1/3} = 0.47$.

The heatline patterns of a $Pr = 0.02$ fluid such as mercury are presented in Fig. 8 (cold wall) and Fig. 9 (hot wall). The heatlines extend well outside the velocity boundary layer shown by the dotted line. They are nearly vertical inside the velocity boundary layer, indicating that convection is not a strong effect so close to the wall. Each heatline was drawn for a round value of the group $\tilde{H}\, Pr^{1/2}$, which is recommended by

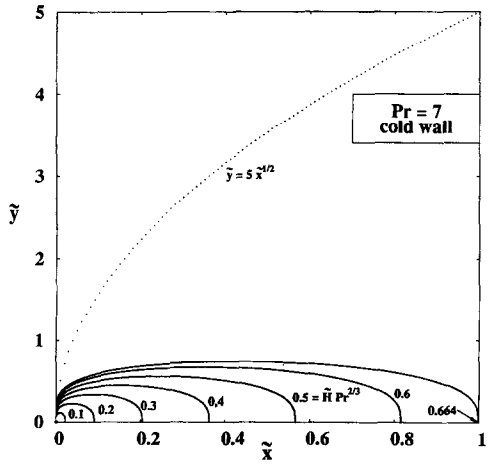

FIG. 6. The heatlines near a cold isothermal wall ($Pr = 7$).

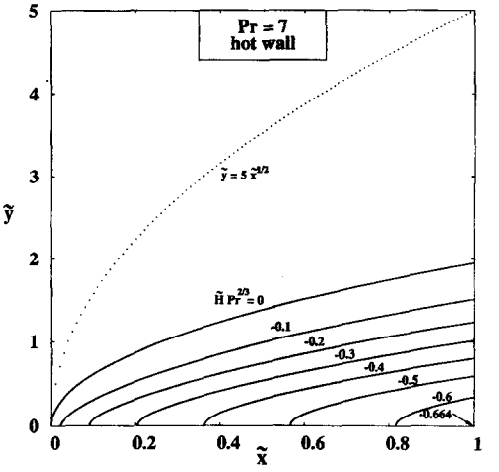

FIG. 7. The heatlines near a hot isothermal wall ($Pr = 7$).

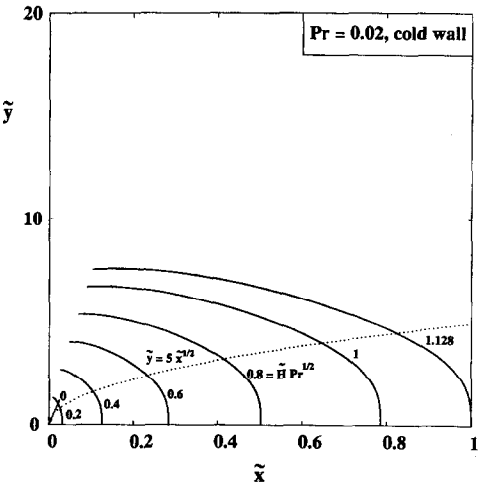

FIG. 8. The heatlines near a cold isothermal wall ($Pr = 0.02$).

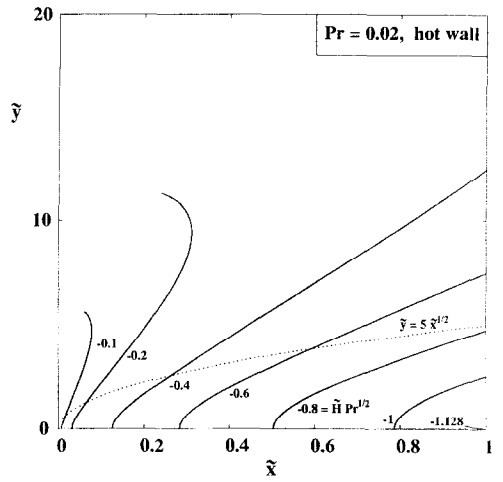

FIG. 9. The heatlines near a hot isothermal wall ($Pr = 0.02$).

equation (22) for the low-Pr range. In this way, the $\tilde{H}\,Pr^{1/2} = 0$ and $\tilde{H}\,Pr^{1/2} = 1.128$ heatlines mark the tip and the trailing edge of the isothermal wall.

6. HEATLINES NEAR A WALL WITH UNIFORM HEAT FLUX

When the heat flux is distributed uniformly over the wall length L, the heatlines will be spaced equidistantly as they enter or exit the wall. This effect can be visualized by plotting the heatlines inside the boundary layer. The analysis is analogous to that of Section 2, except for the temperature distribution in the boundary layer, which is now

$$T(x,y) = T_\infty + \frac{q''}{k}\left(\frac{\nu x}{U_\infty}\right)^{1/2}\theta(\eta). \tag{28}$$

The similarity profile $\theta(\eta)$ is obtained by solving the problem

$$\theta'' + \frac{Pr}{2}(f\theta' - f'\theta) = 0 \tag{29}$$

$$\theta'(0) = -1, \quad \theta(\infty) = 0. \tag{30}$$

The local Nusselt number is

$$Nu = \frac{q''x}{k[T_0(x) - T_\infty]} = \frac{1}{\theta(0)}\,Re_x^{1/2}. \tag{31}$$

We use this opportunity to correct the claim made by Kays and Crawford [9], that a similarity solution does not exist for the constant-flux laminar boundary layer. This claim was questioned earlier by Krane [10]. The similarity solution for the constant-flux problem was reported by Levy [11], Schuh [12] and, as part of a convection and radiation problem, by Sparrow and Lin [13]. The latter reported numerical results for $\theta(0)$ in the Pr range 0.7–100. The $Pr \to 0$ limit of the same problem was reported by Bejan [2] (pp. 358–359, 384–385), who used a finite-difference formulation of the boundary layer near a plane wall swept by parallel flow through a saturated porous medium (see Appendix).

Since our objective was to construct the heat-function inside the thermal boundary layer, we solved equations (29) and (30) numerically for several Pr values. The numerical work began with the observation that the problem of equations (29) and (30) is ill conditioned, since an asymptotic limit is prescribed instead of a principal boundary condition such as $\theta(0)$. Solving equations (29) and (30) using a shooting method (Runge–Kutta) did not yield accurate results, even though convergence was achieved. The lack of accuracy in this case was indicated by the fact that the calculated heatlines were not perfectly perpendicular to the wall.

Instead of shooting we used a finite-difference approach in the finite domain $1 \leqslant \xi \leqslant 0$, where $\xi = 1/(1+\eta)$. The boundary conditions (30) became $\theta = 0$ at $\xi = 0$, and $\theta = 1$ at $\xi = 1$, and in this way we obtained a well posed boundary value problem. We used a nonuniform mesh that allowed enough grid points to accumulate near the $\xi = 1$ boundary. The Roberts transformation [14] effected a second mapping, from $0 \leqslant \xi \leqslant 1$ to $0 \leqslant r \leqslant 1$, bringing the problem to a computational domain with uniform mesh. The discrete operator was constructed using the Kàlnay de Rivas [15] expansions, and the tridiagonal system was solved via the $L\text{-}U$ (Thomas) factorization/backward substitution algorithm. The goodness of the uniform r-meshing was established by monitoring the relative error between the linear and parabolic gradients of θ at the $\xi = 1$ (or $r = 1$, or $\eta = 0$) boundary. A 10^{-4} error limit was imposed and satisfied by adjusting $S = (\partial r/\partial\xi)_{\xi=1}/(\partial r/\partial\xi)_{\xi=0}$ in the range 10^{-1}–10^{-4}. Accuracy tests were performed for grids with nodes varying between 200 and 2000. The reported results correspond to the finest mesh. The solution obtained for $\theta(\eta)$ and $\theta'(\eta)$, which was later used to calculate and plot $\hat{H}(\tilde{x},\tilde{y})$ of equation (37), satisfied also the orthogonality condition $\partial\hat{H}/\partial\tilde{y} = 0$ at $\tilde{y} = 0$.

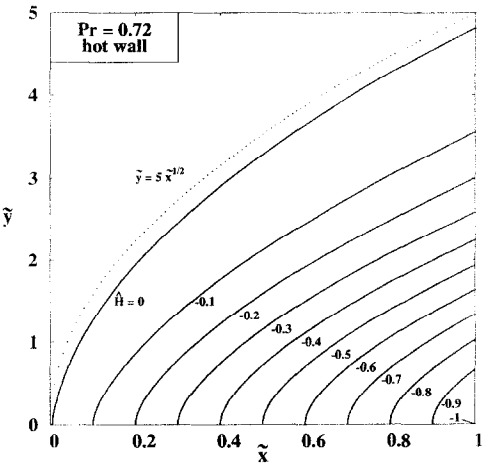

FIG. 10. The heatlines near a hot wall with uniform heat flux ($Pr = 0.72$).

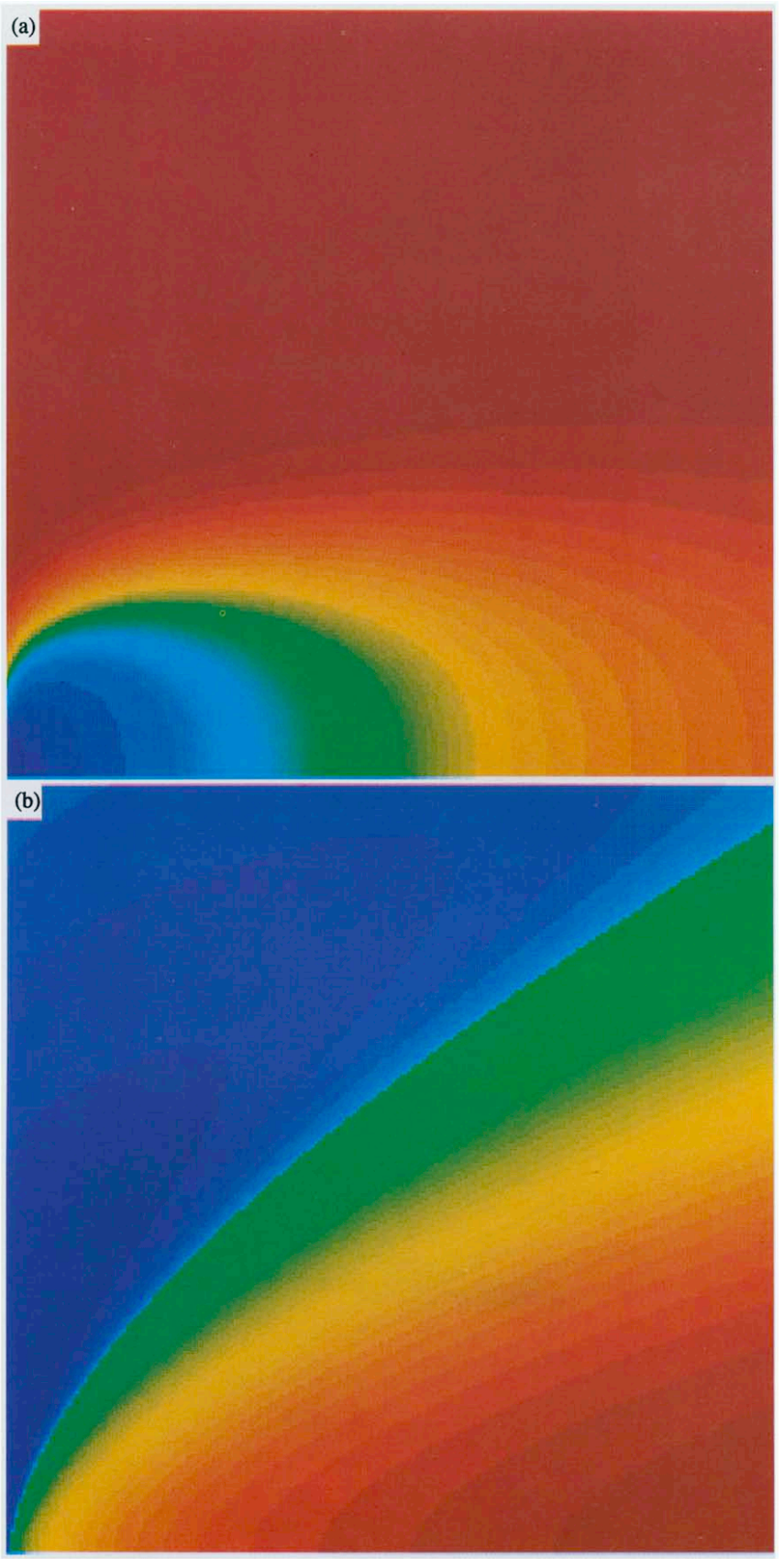

FIG. 11. Color maps of the heatfunctions for a $Pr = 0.72$ fluid near an isothermal wall: (top) cold wall, hot fluid; (bottom) hot wall, cold fluid.

In this way we extended numerically the Sparrow and Lin [13] heat transfer results to Prandtl numbers as low as 2×10^{-4}. These two sets of results behave asymptotically as

$$\frac{1}{\overline{\theta(0)}} = \begin{cases} 0.463\,Pr^{1/3}, & Pr > 10 \\ 0.886\,Pr^{1/2}, & Pr \to 0. \end{cases} \tag{32}$$

We then constructed a compact Nu expression of the Churchill–Ozoe [16] type, which covers the entire Pr range and reproduces all of equations (32),

$$Nu = \frac{0.463\,Pr^{1/3}\,Re_x^{1/2}}{[1+(0.0204/Pr)^{2/3}]^{1/4}}. \tag{33}$$

Finally, we use this as an opportunity to report the derivation of the exact (analytical) expression for the temperature profile and heat transfer rate in the limit $Pr \to 0$, equations (32). This solution is outlined in the Appendix.

The heatfunction $H(x, y)$ follows from equations (4) and (5). We consider the more common situation in which the uniform-flux wall is warmer than the fluid, as in the case of an electrically heated plate. This means that $T_{ref} = T_\infty$. As scale for H we use $q''L$, which is the total (known) heat transfer rate released by the wall,

$$\hat{H}(\tilde{x}, \tilde{y}) = \frac{H(x, y)}{q''L}. \tag{34}$$

Equations (4) and (5) become

$$\frac{\partial \hat{H}}{\partial \tilde{y}} = Pr\,\tilde{x}^{1/2} f'\theta \tag{35}$$

$$-\frac{\partial \hat{H}}{\partial \tilde{x}} = \tfrac{1}{2}\,Pr\,(\eta f' - f)\theta - \theta'. \tag{36}$$

It is not difficult to integrate equations (35) and (36), and to set $\hat{H}(0, 0) = 0$ at the leading edge of the wall to obtain the heatfunction analytically,

$$\hat{H}(\tilde{x}, \eta) = \tilde{x}(\tfrac{1}{2}\,Pr\,f\theta + \theta'). \tag{37}$$

It is worth noting that this heatfunction is of the type $\hat{H} = \tilde{x}g(\eta)$, in which the similarity heatfunction $g(\eta)$ has the same form as in the case of the isothermal wall, equations (16) and (17). This observation stresses the importance of $g(\eta)$, next to the other profiles of the similarity boundary layer, $f(\eta)$ and $\theta(\eta)$.

Since $f(0) = 0$ and $\theta'(0) = -1$, we conclude that the heatfunction decreases linearly along the wall, $\hat{H}(\tilde{x}, 0) = -\tilde{x}$, i.e. that the exiting heatlines are equidistant. Figure 10 shows this feature, along with the heatlines in the immediate vicinity of the wall. This $Pr = 0.72$ figure can be compared directly with Fig. 5 to see the difference between the uniform heat flux and uniform temperature boundary conditions. The heatlines point in the y direction as they come out of the wall: note that since $f' = 0$ at the wall, equation (35) reduces to $\partial\hat{H}/\partial\tilde{y} = 0$.

7. CONCLUSIONS

In this paper we reported in closed form the heatfunctions H for laminar boundary layer flow and heat transfer near a flat wall. The particular form of each heatfunction depends on whether the wall is warmer than the fluid, and on the thermal boundary condition at the wall surface (e.g. uniform temperature, or uniform heat flux). The constant-H lines (the heatlines) can be plotted as soon as the boundary layer velocity and temperature profiles have been calculated.

Since the objective of this study was to visualize the convection phenomenon in the boundary layer region, it pays to review the heat transfer features that are visualized by heatlines, and not by traditional methods such as the use of isotherms:

(a) The path of convective heat transfer from a hot fluid to a cold wall differs totally from the path followed by convection from a hot wall to a cold fluid. Compare, for example, Fig. 3 with Fig. 5.

(b) The energy that is absorbed eventually by a cold wall originates from the fluid that approaches the leading edge of wall. The heatlines then turn and become perpendicular as they enter the wall. Examine, for example, Fig. 3, 6 or 8.

(c) The heatlines of the boundary layer near a hot wall are perpendicular as they exit the wall. Later, they are bent and swept with the flow, while occupying the same region as the thermal boundary layer. This feature is visible in Fig. 5, 7, 9 or 10.

(d) The boundary-layer heatlines are always perpendicular to the wall, regardless of the thermal boundary condition (isothermal vs uniform flux). This feature is an illustration of the fact that the effect of longitudinal conduction has been neglected in the boundary-layer energy equation, by definition of the concept of boundary layer.

(e) The density of the heatlines drawn for constant increments in H can be used to visualize the distribution of heat flux along the wall. Compare the isothermal wall of Fig. 5 with the constant-flux wall of Fig. 10.

In addition to these visualization steps, this study extends to low Pr values the similarity solution for the wall with uniform flux (see the Appendix). A correlation that brings into a single formula the results known for the entire Pr range is proposed in equation (33).

When it is properly nondimensionalized, the heatfunction becomes a spatial generalization of the concept of Nusselt number. We saw that right on the wall the dimensionless heatfunction becomes the same as the classical Nussselt number (e.g. Figs. 3 and 5). More recently, there have been many studies in which the Nusselt number is defined (integrated) along a plane drawn through the convective fluid, for example, through the mid-plane of an enclosure with natural convection (e.g. Lage [17]). In this second kind of Nusselt number the heat transfer rate is cal-

culated as a superposition of convection and conduction, in the same way as in the construction of H. The heatfunction is a 'spatial' generalization of the Nu concept, in the sense that it describes the magnitude and direction of the heat transfer rate through any surface that can be imagined inserted in the convective medium.

We conclude this visualization study with Fig. 11, which shows the color maps of the heat functions calculated for a $Pr = 0.72$ fluid. The color red means hot, and blue means cold. These maps correspond to the heat line patterns of Figs. 3 and 5, and illustrate once again the difference between a wall that serves as heat sink (Fig. 11, top) and one that serves as heat source (Fig. 11, bottom).

Acknowledgement—This study was made possible by a grant from the North Carolina Supercomputing Center. The special advice and assistance provided by Mr Jeff Knerr is very much appreciated.

REFERENCES

1. S. Kimura and A. Bejan, The "heatline" visualization of convective heat transfer, *J. Heat Transfer* **105,** 916–919 (1983).
2. A. Bejan, *Convection Heat Transfer*, pp. 21–23, 450–452. Wiley, New York (1984).
3. D. Littlefield and P. Desai, Buoyant laminar convection in a vertical cylindrical annulus, *J. Heat Transfer* **108,** 814–821 (1986).
4. O. V. Trevisan and A. Bejan, Combined heat and mass transfer by natural convection in a vertical enclosure, *J. Heat Transfer* **109,** 104–109 (1987).
5. Al. M. Morega, The heat function approach to the thermo-magnetic convection of electroconductive melts, *Rev. Roum. Sci. Techn.-Electrotechn. et Energ.* **33**(4), 359–368 (1988).
6. S. K. Aggarwal and A. Manhapra, Use of heatlines for unsteady buoyancy-driven flow in a cylindrical enclosure, *J. Heat Transfer* **111,** 576–578 (1989).
7. C. J. Ho and Y. H. Lin, Natural convection of cold water in a vertical annulus with constant heat flux on the inner wall, *J. Heat Transfer* **112,** 117–123 (1990).
8. A. Bejan, *Heat Transfer*, p. 238. Wiley, New York (1993).
9. W. M. Kays and M. E. Crawford, *Convective Heat and Mass Transfer* (2nd Edn), p. 151. McGraw-Hill, New York (1980).
10. R. J. Krane, Private communication to A. Bejan, Florence, Italy (1990).
11. S. Levy, Heat transfer to constant-property laminar boundary-layer flows with power-function free-stream velocity and wall-temperature variations, *J. Aero. Sci.* **19,** 341–348 (1952).
12. H. Schuh, On asymptotic solutions for the heat transfer at varying wall temperatures in a laminar boundary layer with Hartree's velocity profile, *J. Aero. Sci.* **20,** 146–147 (1953).
13. E. M. Sparrow and S. H. Lin, Boundary layers with prescribed heat flux—application to simultaneous convection and radiation, *Int. J. Heat Mass Transfer* **8,** 437–448 (1965).
14. G. O. Roberts, Computational meshes for boundary layer problems. *Proc. Second Int. Conf. Numerical Methods in Fluid Dynamics, Lecture Notes in Physics* (Edited by M. Holt), Vol. 8, pp. 171–177. Springer-Verlag, Berlin (1970).
15. E. Kàlnay de Rivas, On the use of nonuniform grids in finite-difference equations, *J. Comp. Phys.* **10,** 202–210 (1972).
16. S. W. Churchill and H. Ozoe, Correlations for laminar forced convection with uniform heating in flow over a plate and in developing and fully developed flow in a tube, *J. Heat Transfer* **95,** 78–84 (1973).
17. J. L. Lage, Effect of the convective inertia term on Bénard convection in a porous medium, *Numer. Heat Transfer, Part A* **22,** 469–485 (1992).

APPENDIX. EXACT SOLUTION FOR THE THERMAL BOUNDARY LAYER ON A FLAT PLATE WITH UNIFORM HEAT FLUX WHEN $Pr \to 0$

If we set Pr equal to zero, the similarity temperature boundary layer problem (28)–(30) is replaced by

$$T(x,y) = T_\infty + \frac{q''}{k}\left(\frac{\alpha x}{U_\infty}\right)^{1/2}\tau(\zeta) \tag{A1}$$

$$\zeta = y\left(\frac{U_\infty}{\alpha x}\right)^{1/2} \tag{A2}$$

$$\tau'' + \tfrac{1}{2}(\zeta\tau' - \tau) = 0 \tag{A3}$$

$$\tau'(0) = -1, \quad \tau(\infty) = 0. \tag{A4}$$

Separation of variables is achieved by differentiating equation (A3) once,

$$\frac{\tau'''}{\tau''} = -\tfrac{1}{2}\zeta. \tag{A5}$$

This equation is then integrated sequentially three times, and, after using equations (A3) and (A4), the analytical expression for the similarity temperature profile becomes

$$\tau(\zeta) = \frac{2}{\pi^{1/2}}\exp\left(-\frac{\zeta^2}{4}\right) - \zeta\,\mathrm{erfc}\left(\frac{\zeta}{2}\right). \tag{A6}$$

This shows that the value at the wall is $\tau(0) = 2/\pi^{1/2}$. On the other hand, by comparing equations (28) and (A1) for $T = T_0$, we find that $\tau(0) = Pr^{1/2}\theta(0)$. In conclusion, the low-Pr asymptote listed in equations (32) is actually

$$\frac{1}{\theta(0)} = \frac{Pr^{1/2}}{\tau(0)} = \frac{\pi^{1/2}}{2}Pr^{1/2} \tag{A7}$$

where $\pi^{1/2}/2 = 0.886$. This numerical result (0.886) is the same as the value produced by the finite-difference numerical treatment of the same boundary layer problem (Bejan [2], p. 358).